Biogeotechnics 4 (2026) 100197

Contents lists available at ScienceDirect

Biogeotechnics

journal homepage: www.keaipublishing.com/en/journals/biogeotechnics/

3D printing lunar regolith simulant with microbial-carbonated magnesium oxide

Hanlong Liu[a,b], Yang Xiao[a], Jinquan Shi[c,*], Baofeng Cao[a], Junbo Sun[b]

[a] School of Civil Engineering, Chongqing University, Chongqing 400045, China
[b] Institute for Smart City of Chongqing University in Liyang, Chongqing University, Liyang 213300, China
[c] Department of Civil and Environmental Engineering, The Hong Kong University of Science and Technology, Hong Kong 999077, China

ARTICLE INFO

Keywords:
Lunar regolith simulant
3D printing
Biocarbonation
Magnesium oxide

ABSTRACT

Lunar construction is important and a challenge for building space habitation. Several technology routines using in-situ lunar regolith as the base material for making lunar bricks have been proposed but they are still waiting in the list of verification. In this study, a new additive manufacturing method for making lunar regolith structures with biocarbonated magnesium oxide (MgO) was proposed. A lunar regolith simulant (LRS) was prepared. The effects of microbial-based prehydrolyzed urea solution, additives, and aggregates, on the properties of 3D printing mortars were investigated. The compressive strength and microscopic images of 3D printed specimens were analyzed. The test results showed that the microbial-based mortar has significantly different flowability and buildability compared with water-based mortar. The compressive strength of 3D printed specimens can be improved several times with the biocarbonated method. Microscopic images showed that the printed biocarbonated specimens show denser structure and more magnesium carbonate hydrate, causing the improvement of mechanical behavior. Complex LRS-based structures were printed with the biocarbonated magnesium oxide method, which can bear a certain of loads.

1. Introduction

With the ongoing breakthrough of space technology, lunar exploration has become reliable for regions and countries (Zheng et al. 2008). Lunar is seen as an important transferring base for human's step toward deep places in the universe (Crawford et al. 2012). By exploiting the resources, such as rare metals and helium-3, on the Moon, interstellar travelling could be achieved and the risk of resource exhaustion on the earth can be relieved (Ding et al. 2023). For sustainably maintaining activities on the Moon, building lunar human base with in-situ resources is the inevitable part and has attracted extensive attentions in academic and industry (Ellery, 2021; She et al., 2025; Zhou et al., 2019; Zhou et al., 2025). Using lunar regolith for lunar construction is one challenging task and has been studied for decades (Benaroya et al., 2002; Nie et al., 2025; Pederson et al., 2025). Several routines with technical feasibility, focusing on lunar regolith molding, were proposed (Bao et al. 2024). However, all the methods are still in the conceptual or research stage since the practical application on the Moon is still propelling for most countries and companies.

Lunar regolith molding methods can be classified into several categories, such as sintering, bonding and constraining (Bao et al. 2024). The sintering method is to melt lunar regolith under the high temperature of around 1000 ℃ in precasted mold or with additive manufacturing (Ge et al., 2025; Han et al., 2022; Meurisse et al., 2018; Osio-Norgaard et al., 2021; Zhou et al., 2019). Extensive studies have been carried out to investigate the factors affecting the performance of sintered specimens, such as particle size gradation of regolith simulant (Indyk and Benaroya, 2017), mineral of regolith simulant (Meurisse et al. 2017), regolith density (Zhang et al. 2021b), sintering temperature (Warren et al. 2022), sintering environment (Indyk and Benaroya, 2017), among others. Most of the studies used basalt to make the LRS based on the current real samples taken from Mare regions (Song et al., 2020; Taylor et al., 2016). Therefore, we can see that the morphology of the sintered specimens exhibits dark black color. The strength of the sintered specimens can reach over 200 MPa which is comparably higher than the molded specimens with other methods (Indyk and Benaroya, 2017). Bonding method for casting lunar regolith varies with the bonding materials that can be cement (Neves et al. 2020), sulphur

* Corresponding author.
E-mail address: jinquan_shi@163.com (J. Shi).

https://doi.org/10.1016/j.bgtech.2025.100197
Received 22 June 2025; Received in revised form 16 July 2025; Accepted 30 July 2025
Available online 5 August 2025
2949-9291/© 2026 The Authors. Publishing services by Elsevier B.V. on behalf of KeAi Communications Co. Ltd. This is an open access article under the CC BY license (http://creativecommons.org/licenses/by/4.0/).

(Shahsavari et al. 2022), magnesium oxide (Osio-Norgaard et al. 2021), epoxy resin (Bao et al. 2025), alkali-activator (Ma et al., 2023; Pederson et al., 2025), and biobased binders (Shi et al. 2024). This method mostly relies on the Earth-based materials. For example, alkali-activator like sodium silicate and sodium hydroxide, epoxy resin and Portland cement can not be sourced from Moon and must be transported from earth. Some studies disclosed that magnesium oxide can be extracted from olivine with acid leaching (Scott et al. 2021). The mineral composition of real lunar regolith shows a certain amount of olivine and can be used for producing magnesium oxide. Besides, some studies suggested magnesium phosphate cement as the binder for lunar construction since it requires a lower demand of water for casting (Li et al. 2025). It is still challenging to find a binder material which can be independently sourced or regenerated on Moon. Recently, studies proposed that bacteria might be used for extraterrestrial living support, including habitation construction. The mycelium and microbially induced calcium carbonate precipitation (MICP) could be the two choices (Dikshit et al., 2021; Liu et al., 2023a). For example, MICP and biocarbonated magnesium oxide can be used to make lunar regolith bricks (Shi et al. 2024).

For constructing lunar habitat, 3D printing is deemed as a feasible way since it has the advantage of automatic control and can meet the requirement of building shape which suits the lunar environment (Ulubeyli, 2022). Depending on the processing technique, 3D printing with lunar regolith can be classified as extrusion printing, powder bed printing and sintering printing (Ulubeyli, 2022). Extrusion and powder bed 3D printing requires mixing lunar regolith with binders and water, such as cement and alkali-activator. It was reported ice might distribute in the polar area of the Moon (Cocks et al. 2002). The two methods are also restricted by the binder material resources since producing cement-based or magnesium-based binders is still a technical challenge currently. Sintering 3D printing uses solar or laser energy to sinter lunar regolith layer by layer. The key parameters for maintaining printing quality involve solar energy collection, sintering temperature control, and porosity control of the printed specimen, among others (Bao et al., 2024; Han et al., 2022; Meurisse et al., 2017). Meurisse et al. (2018) performed laboratory sintering tests using solar energy to make LRS bricks. They found that the printed specimens show a low compressive strength of about 5 MPa, which is caused by the high porosity and the weak bonding between layers. The process can be optimized by changing the thermal gradient and cooling time during printing. Nakamura and Smith (2011) reported a field testing of sintering 3D printing with a volcanic ash and the technical details involving solar concentrator array, power system assembly and operation, were given. The output power measurement and the effects of dust on the inlet optics were analyzed. The filed tests verified the feasibility of using solar energy to conduct the lunar regolith 3D printing construction.

For the binder-based lunar regolith 3D printing, Ma et al. (2023) performed 3D printing testing focusing on the composite structures of LRS using alkali activation method. The strength of the composite with bioinspired structure vary with the structure type and the maximum compressive strength can reach around 20 MPa. Osio-Norgaard et al. (2021) used magnesium oxychloride cement as the binder to print structures with regolith simulant for sintering. Jetting method was employed, with which complex structure printing was achieved. Bao et al. (2025) tested the 3D printed composites with the resin-based lunar regolith ink. With the freeze-thaw tests, they found that the composites have high resistance to temperature and show good performance for construction purpose.

Microbial was seen as the potential media for lunar habitat construction and human living. How to use microbial-based binders to bond lunar regolith and improve the strength improvement efficiency is still the concern for research. Shi et al. (2024) proposed to use biocarbonated magnesium oxide binder to make lunar regolith biobricks. Compared with pure magnesium oxide, the strength can be improved more than 8 times. This method can save magnesium oxide which can be sourced from olivine in regolith with the acid leching method (Scott et al. 2021). Besides, microbial can be cultured with the kitchen residual and the human or animal urine can provide urea. In this study, 3D printing is employed to make composites with lunar regolith mortar combined with microbial-carbonated magnesium oxide binders. The flowability and green strength of the microbial-based mortar are tested. The compressive and flexural strength is examined to evaluate the anisotropic strength of the printed specimens.

2. Materials and methods

2.1. Lunar regolith simulant

Several countries have taken samples from Moon and the data of lunar regolith morphology, particle size gradation, chemical and mineral composition was reported extensively (Li et al., 2022; Nie et al., 2025; Papike et al., 1982; Taylor et al., 2016; Zhang et al., 2021a). To prepare the LRS used for this study, particle size gradation, chemical composition and morphology were mainly considered (Zhang et al. 2021a). The volcanic rock from Inner Mongolia volcanic group was ground to the ash with the particle size gradation shown in Fig. 1C. The chemical component is shown in Table 1. It is seen that the particle size is a little bit finer than the typical particle size of lunar regolith. The most significant difference in chemical components between the simulant and the real regolith is ferric oxide. It was reported that ferric oxide in Chang'e-5 sample is higher than that in Apollo soils (Li et al. 2022). Considering the chemical properties of the minerals are stable and should not affect the biocarbonation process in this study, the difference in ferric oxide is neglected. However, this can be solved by adding ilmenite to the basic materials. In Fig. 1D–F, the particle shape parameters, aspect ratio, sphericity, and convexity, of the simulant were compared with the data of real lunar soils measured in (Nie et al. 2023). The morphology data was obtained with a dynamic particle image analyzer QICPIC. We see that the simulant used in this study show slightly higher angularity than the real lunar soils, reflected by the larger aspect ratio and convexity and lower sphericity. This may cause different mechanical behavior of 3D printed specimens since a higher irregularity cause higher compressive strength for biocemented sands (Xiao et al. 2019). In this study, the effect of lunar regolith morphology will not be included. To investigate the effects of aggregate on the strength and printability, a machine sand replacing coarse lunar regolith, with the diameter ranging from 0.3 to 0.5 mm, were used in this study. The additive, such as hydroxymethyl cellulose and commercial retarder, were chosen for optimizing printability of the microbial-regolith mortar.

2.2. Bacterial-hydrolyzed solution preparation

For preparing the biocarbonated solution, Sporosarcina pasteurii was selected as the bacteria for urea hydrolysis. Bacteria was stepwise scale-up cultured from 600 mL to 6000 mL and the culture the medium consists of 20 g/L yeast extract, 15 g/L ammonium chloride, 1 ml/L nickel chloride solutions with the concentration of 0.1 mol/L. 600 mL bacterial solutions were cultured with a shaking incubator under the temperature of 30 degree celsius for 8 h. Then the solutions were transferred to a container with 5400 mL medium. An air pump in a fume cupboard supplied air via connecting four bubble stones at the bottom of the container and the culturing time lasted around 10 h. In this process, temperature is not controlled and the propagation was kept at ambient temperature at around 21 degree celsius. The hydrolysis activity was examined via hydrolyzing 18 mL urea solution with 1.1 mol/L with 2 mL bacterial solution and the electricity conductivity larger than 0.1 mS/cm/min was deemed to be usable. OD600 of bacterial solutions were examined before they were used for pre-hydrolysis during which the urea solutions of 2 mol/L were mixed with the bacterial solution at equal volumes. In this paper, OD600 was controlled at

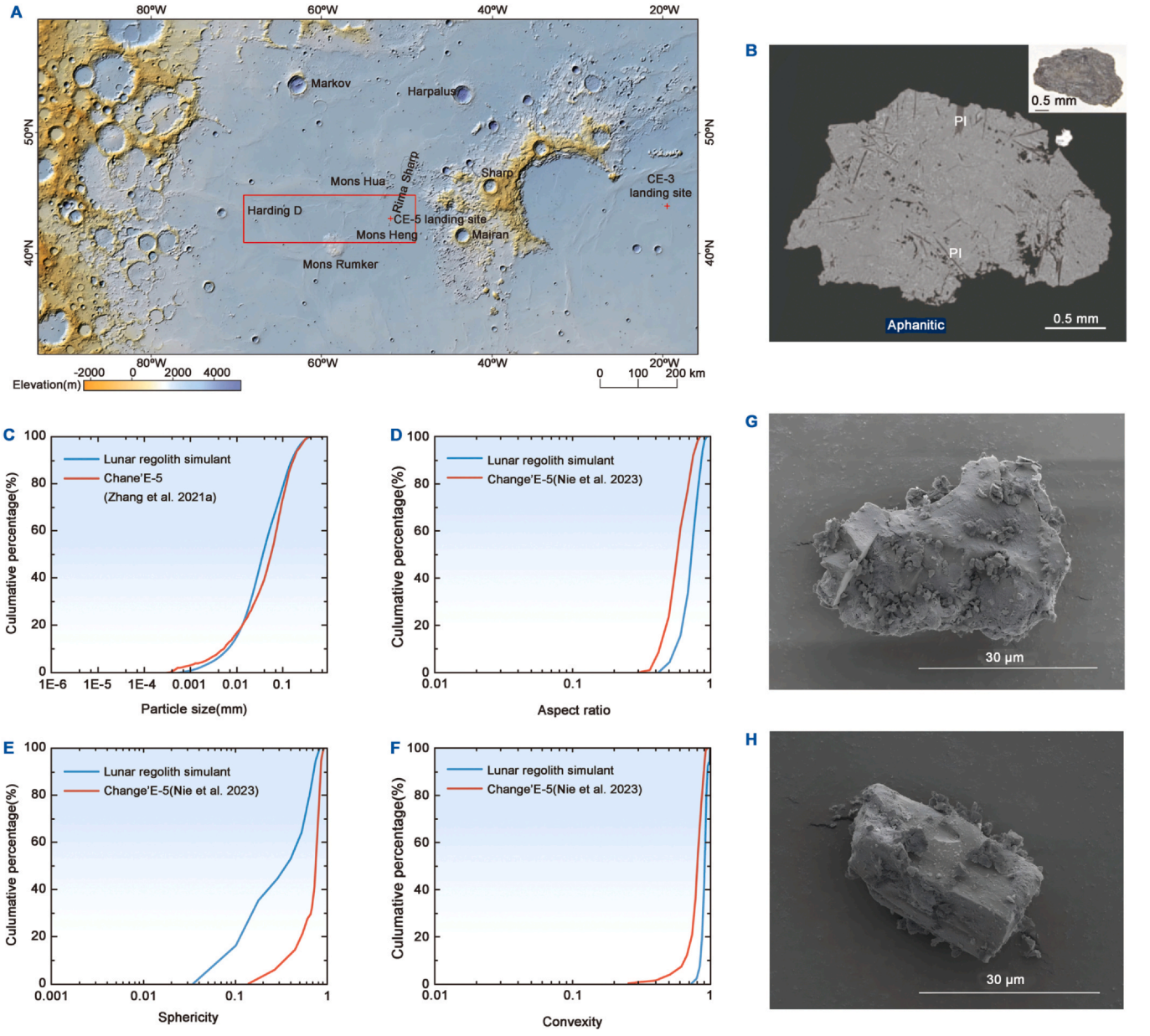


Fig. 1. Particle size gradation and particle shape parameters of LSR: (**A**) Collection position of Chang'e-5 lunar soil sample (Li et al., 2022); (**B**) Particle morphology of Chang'e-5 lunar soil sample (Li et al., 2022); (**C**) Particle size gradation of LRS and Chang'e-5 lunar sample (Zhang et al., 2021a); (**D–F**) Particle shape parameter of LRS and Chang'e-5 lunar sample (Nie et al., 2023); (**G–H**) Particle morphology of LRS.

around 1.6. For each test, a total of 12 L hydrolyzed solution was prepared and the electricity conductivity was measured at around 84 mS/cm at each end of hydrolysis.

2.3. Flowability test of microbial lunar regolith mortar

Flowability is critical for 3D printing mortar. Here, we used slump flow test to investigate the effects of hydrolysis solution, magnesium oxide content, aggregate content, retarder and thickener on the flowability of regolith mortar. The tests were performed according to the Chinese standard for testing fluidity of cement mortar (GB/T 2419-2005). A hollow mold with top and bottom diameters of 70 mm and 100 mm and a height of 60 mm was used. Firstly, mortar was filled 2/3 of the mold height and tamped with a steel bar in a circular routine for 15 times. After scratching the surface of the filled mortar, the mold was filled and tamping was performed 10 times for the second layer. The

Table 1
Chemical component of lunar regolith simulant and data from literature.

Component(%)	SiO_2	FeO_x	Al_2O_3	CaO	MgO	TiO_2	K_2O	P_2O_5	MnO	Na_2O	Total
Simulant	46.95	14.59	13.62	10.25	6.73	3.29	2.85	1.18	0.24	0.13	99.83
Chang'e−5	42.2	22.5	10.8	11	6.48	5.00	0.19	0.23	0.28	0.26	98.94

Note: The chemical component of Chang'E-5 lunar regolith references the data from Li et al. (2022)

Table 2
Test program.

Group	MgO/regolith	Water/binder	Bacterial/binder	HMC/binder	Retarder/binder	Aggregate/binder	Test Type
G−1	0.2	0.34	-	0.1	0.2	0	F, C
G−2						0.5	F, C, G
G−3						1	F, C
G−4		-	0.34	0.1	0.2	0	F, C
G−5				0.1	0.2	0.5	F, C, G
G−6				0.1	0.2	1	F, C
G−7				0	0.2	0.5	F, C
G−8				0.2	0.2	0.5	F, C
G−9		0.42	-				F
G−10		0.4	-				F
G−11		0.37	-				F

Note: the ratio in this table is calculated by mass; the binder here means the mixture of regolith and MgO; F. Flowability test, C. Compressive test, G. Green strength test; aggregate is sand.

final height of mortar was slightly higher than the mold height and was levelled with a scrapper. The mold was lifted slightly and the table was started with jumping frequency of 1 time/s for 25 s. Finally, the diameter of the mortar was measured two times perpendicularly. The whole process of the test should be completed within 6 mins.

2.4. Green strength tests

For examining the initial strength of the lunar regolith mortar, green tests were performed on the fresh mixtures in the first 4 h from mixing. The specimens were prepared in a split mold and the mortar was filled in the mold with 3 layers. Due to the quite low strength of the mortar at the beginning, the specimens can not stand by itself and the first test started from the 50th min after mixing. The specimens were compressed in a universal machine equipped with a load 5kN load cell and the loading rate was set at 0.1 mm/s. The strength was measured at the time of 50 min, 90 min, 120 min, 190 min, 240 min. The effects of solution type and aggregate on the green strength of the mortar were examined.

2.5. 3D printing tests

A large-scale 3D printing machine with the length of 2.5 m, the width of 2.5 m and the height of 2 m was used in this study. The mortar was manually filled into an extruder which is capable of controlling the extrusion speed and moving speed. The geometry was designed and sliced as G-code files before printing. In the 3D printing stage, the LRS was stirred with magnesium oxide, retarder and thickener before water or bacterial-hydrolyzed solution was added. The mixing process lasted around 1 min for binders and 4 mins after solutions were poured. A single layer wall was firstly designed and printed to examine the buildability of mixture. The maximum stacked layers, wall height and the width of each

layer was compared considering the effects of water/binder ratio, solution type, aggregate and additives. For testing the compressive and splitting strength of the 3D printed composite, the bricks with the approximate dimensions of 200 mm in length, 150 mm in width and 7 cm in height were printed with the nozzle size of 15 mm in diameter and printing speed of 50 mm/s. The 28-day strength of the specimens, segmented at the 14th day after printing, were tested and the anisotropic mechanical behavior, involving shear wave velocity, was analyzed. The microscopic structure of the printed specimens was examined using scanning electron microscopy (SEM) methods. The cubic specimens with the dimension of 40 mm × 40 mm × 40 mm were used for CT scanning. The test program was shown in Table 2 and the test flow diagram is shown in Fig. 2.

3. Test results

3.1. Flowability test

The results of jump table tests were shown in Fig. 3. The averaged diameters measured in the tests were plotted and the effects of solution type, water/binder ratio, HMC content, retarder content and resting time were considered. In Fig. 3A, it is obvious that the flow diameters increase with the increase of W/B ratios. The water can improve the flowability of 3D printing mortar. However, for magnesium-based cementing materials, the strength decreases with the increase of W/B

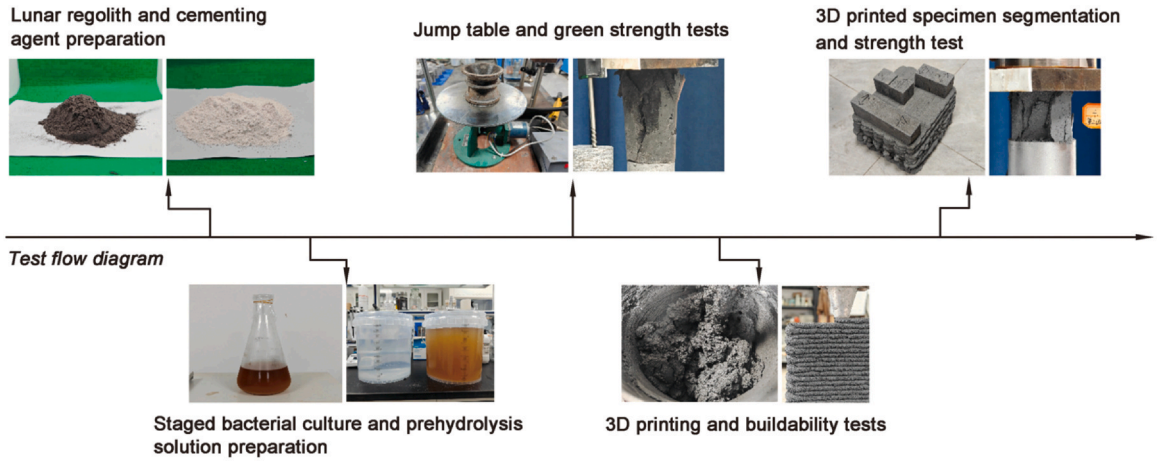


Fig. 2. Testing diagram.

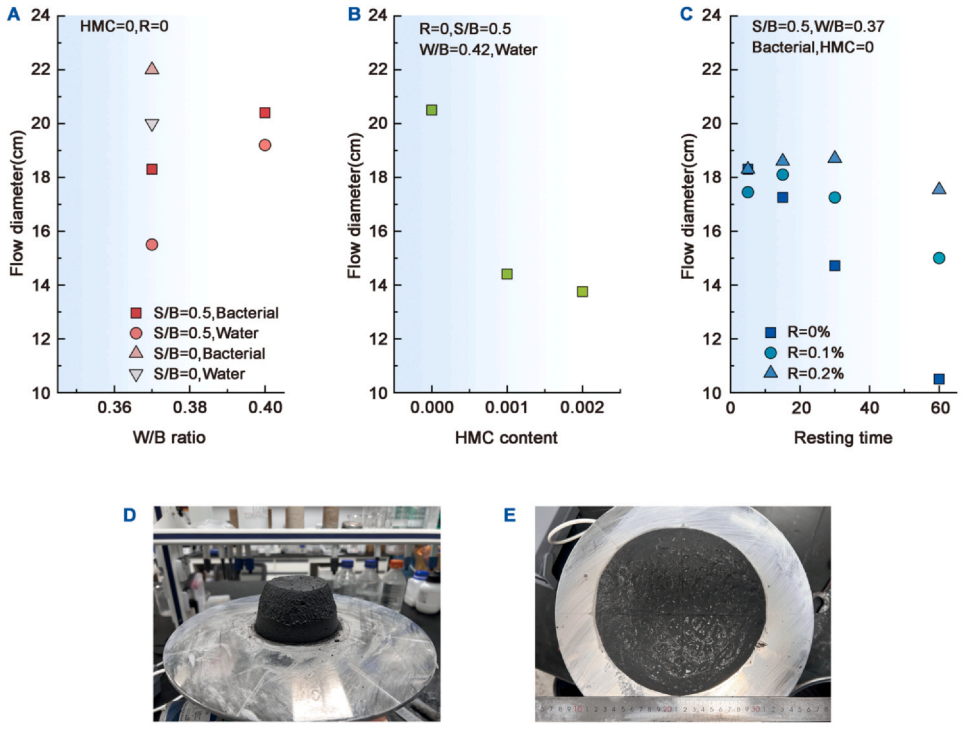


Fig. 3. Diagram of flowability test: (**A**) Effect of water/binder ratio; (**B**) Effect of HMC content; (**C**) Effect of resting time; (**D**) Specimen before jump table test; (**E**) Specimen after jump table test.

ratio, which is caused by the difference in hydration compound (Buj et al. 2009). Besides, the flow diameters of the mortars with bacterial solution are significantly higher than those prepared with water. This is caused by the phenomenon called electrostatic repulsion as reported by Su et al. (2019). In their study, bacterial solution with negative surface charge absorbs positive calcium ions, forming positive particles. The positive particles can be integrated into the diffusion layer around cement particles, increasing the electrostatic repulsive force of the matrix. This phenomenon induces the increase of flowability of the mortar. In this study, the bacterial hydrolyzed urea and the solution contained bacterial, ammonium ion and carbonate ion. The increase in conductivity of hydrolyzed solution was mainly caused by the exist of ammonium and carbonate ions. Based on the hydrolysis equation, the amount of ammonium ions could be twice more than carbonates since ammonia is more soluble in water compared with carbonate dioxide. In the stage of mortar preparation, MgO reacting with water generates magnesium ions and hydroxyl ion. Therefore, MgO particles absorbing more ammonium ions and bacterial formed positive particles. These particles adhered on the grains of LRS, increasing the electrostatic repulsive force of the mortar. This explained why the bacterial mortar shows higher flowability compared the mortar prepared with water.

HMC is commonly used to improve the cohesion and viscosity of 3D printing mortar (Chen et al. 2020b). Since there is still no international standard introducing the use of HMC for 3D printing technique, it has been investigated extensively in prior studies and the effects of HMC dosage and type as well as the working mechanism were reported (Li et al., 2018; Reiter et al., 2018; Shoaei et al., 2024). In this study, due to the weak ability in retaining water of LRS, adding thicker to the mortar is essential for improving the poor extrudability and shape stability, as shown in Fig. 3C. In Fig. 3D, the effect of HMC content on the flowability of the bacterial-based mortar was exhibited. It is seen that with addling of HMC, the flow diameter significantly decreases. The decrement reduces when the HMC contents changes from 0.1% to 0.2%. Based on the observation during testing, 0.2% HMC changes the viscosity of the mortar significantly, which makes mortar stick on the extruder. Li et al. (2018) recommended the optimal dosage of HMC is around 0.15%. But Chen et al. (2020b) reported that 0.24% is the suitable content for their 3D printing tests. In the subsequent tests, the printed specimens with 0.1% and 0.2% HMC will be compared in the aspect of strength and microstructure.

For the mortar with bacterial-based solution, the setting time should be short since the rich content of carbonate in the prehydrolysis solution can accelerate the hydration reaction of MgO (Liu et al., 2024; Ma et al., 2020). For prolonging the setting time of 3D printing mortar, retarder is always adopted in prior studies (Chen et al. 2020b). In this study, a commercial retarder was used for regulating the setting time of bacterial-based lunar regolith mortar. The flow diameters with the change of retarder content and testing time were measured. It is seen that for the mortar without retarder, the flow diameter drops to around 10 mm at 60th min. This means the mortar is not suitable for 3D printing. With the observation during tests, the mortar becomes quite hard at around the 50th min and can not be extruded. The nozzle was blocked due to the poor flowability of the mortar. With the addition of retarder, the flowability of the mortar is significantly improved. A dosage of 0.2% keeps the flow diameter at around 17.54 mm at the 60th min, which is slightly lower than the initial value. Besides, it is noted that the flow diameters slightly increase at the 15th min for the mortar with 0.1% and 0.2% retarder. This illustrates that retarder can not only prolong the setting time, but also increase the flowability in the initial stage. The main component of the retarder is calcium gluconate. Gluconate ions can combine with Mg^{2+} on the surface of MgO to prevent the hydration. Once the gluconate ions are entirely consumed, the hydration will be accelerated again (Tramontin Souza et al. 2022). This process induces more free water in the mortar, leading to the slight increase of flow diameter at the initial stage (Chen et al. 2020a). More retarder can prolong this process and this can be seen in Fig. 3, that the flow diameter starts decreasing at the 30th min for the dosage of 0.2%.

3.2. Green test

In Fig. 4, the green test results are exhibited and the effects of aggregate, setting time, and solution type on the strength and deformation

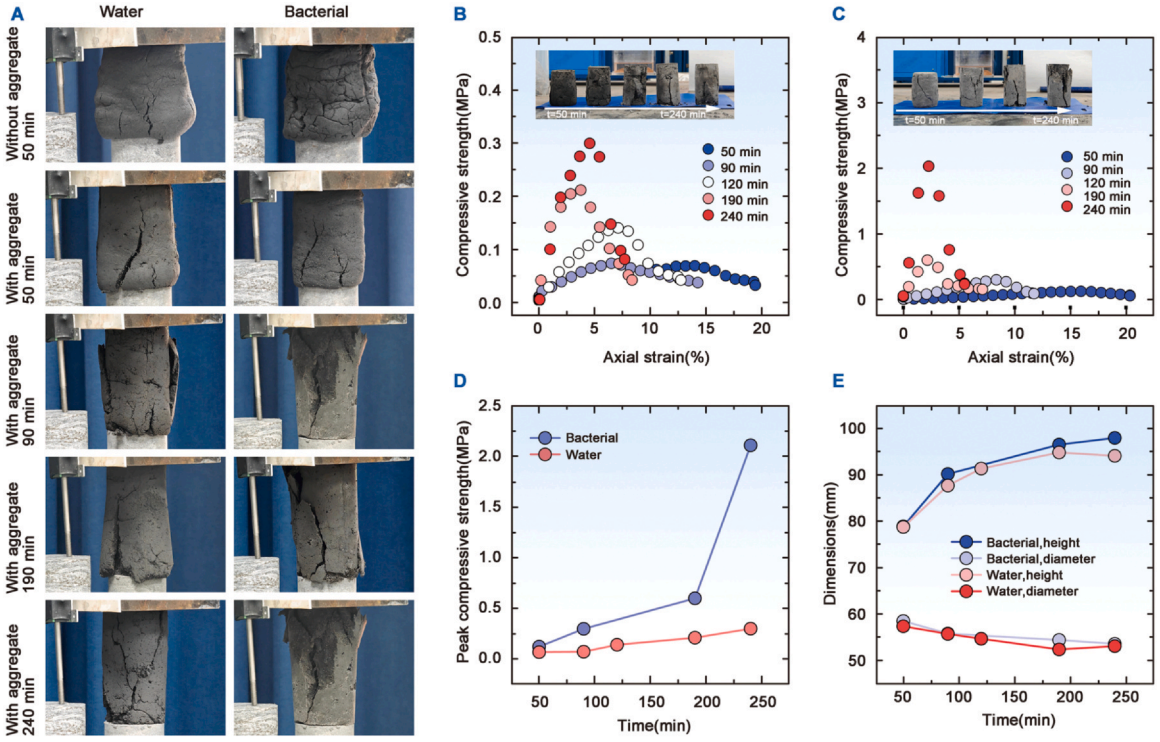


Fig. 4. Green strength test: (**A**) Failure morphology of specimens at different testing time; (**B**) Green strength-strain curves of water-based specimens at different resting time; (**C**) Green strength-strain curves of bacterial-based specimens at different resting time; (**D**) comparison of peak strength between water-based and bacterial-based specimens; (**E**) Dimension of specimens at failure.

of the green specimens are investigated. The specimens were prepared with 0.2% retarder and 0.1% HMC. The morphology of the specimens at the end of loading is shown in Fig. 4A. It is seen that without aggregate, the specimens exhibit twisty pattern. This is due to that the initial strength is too low to hold the self-weight of the specimens even at the 50th min. The degree of distortion is more serious for the bacterial-based specimen. This is because that the higher flowability of the mortar containing bacterial-solution, as explained above. With the addition 50% aggregate by weight, the buildability of the specimens is improved significantly. The deformation becomes less ductile. Bai et al. (2021) showed that aggregates play important roles in strengthening skeleton and improving the buildability of 3D printing mortar. With the increase of setting time, it is seen that the structure of the specimens is more and more significant. At the end of 240th min, splitting failure was observed, indicating the specimens have gained enough strength.

The UCS curves of these specimens were shown in Fig. 4B and C. The peak strength increases with setting time and the axial strain corresponding the peak strength decreases. The bacterial-based specimen shows the maximum peak strength of around 2.11 MPa at the 240th min. In Fig. 4D, the peak compression strength of bacterial-based specimens increases hugely after 190th min. This means that the effect of retarder on the hydration reaction of MgO is mitigated. For the water-based mortar, the strength development is progressive even after 190th min. The data of specimen deformation is summarized in Fig. 4E. The diameters were measured at the middle of specimens for three times and the average was used. It is seen the diameters of specimens after failure continuously drop with the setting time. The variation of specimen height shows an inverse trend. This is consistent with the observation of the morphology development of green specimens under compression.

The buildability of lunar regolith mortar was examined via printing a single layer wall and the printed height and width were recorded. Fig. 5A shows the patterns of printed wall considering the factors of setting time and HMC. For the mortar without HMC, significant cracks were observed on the surface for each layer. This is due to that the low cohesion between binder particles. The addition of HMC improves the viscosity and cohesion of the mortar to resistance the surface tension and leads to the smooth surface of the printed parts. This is also exhibited by the comparison of printed bricks with and without HMC in Fig. 5. In Fig. 5A, the pattern of the wall within and exceeding setting time is shown. In order to extrude the mortar exceeding setting time of 240 min, the extrusion speed was adjusted to 150 mm/s. This leads to discontinuous and inhomogeneous filament and the bonding between layers is quite weak. However, within the setting time, homogeneous layers were printed and the connection between each layer was improved. Fig. 5B and C, the specific change of layer dimension with setting time and extrusion speed is exhibited. It is seen that the height and width of the printed wall increase and decrease with setting time, respectively. With the increase of extrusion speed, the stacked layer number, wall height and wall width increase. This illustrates that the increase of layer width can improve the buildability due to the increase of stability of the printed structure.

3.3. Compressive strength tests

In order to examine the strength of the 3D printed LRS, the printed block was segmented into smaller cubic with the dimension of 40 mm. The comprehensive strength was shown in Fig. 6. The factors, such as aggregate content, HMC content, and the comparison between water and bacterial solutions were investigated. From Fig. 6A, B and D, it is interesting to see that the effect of aggregate content plays different roles in the water-based and bacterial-based specimens. For water-based specimens, compressive strength decreases with the decrease of aggregate content. The overall compressive strength is lower than 2.5 MPa. However, for the bacterial-based specimens, the strength increase with the content of aggregate is reduced. The maximum strength of the bacterial-based specimens is 11.136 MPa, in which no aggregate is added. The two different development trends in specimen

strength is probably due to the different working mechanism of cohesion strength between aggregate and binder. The strength

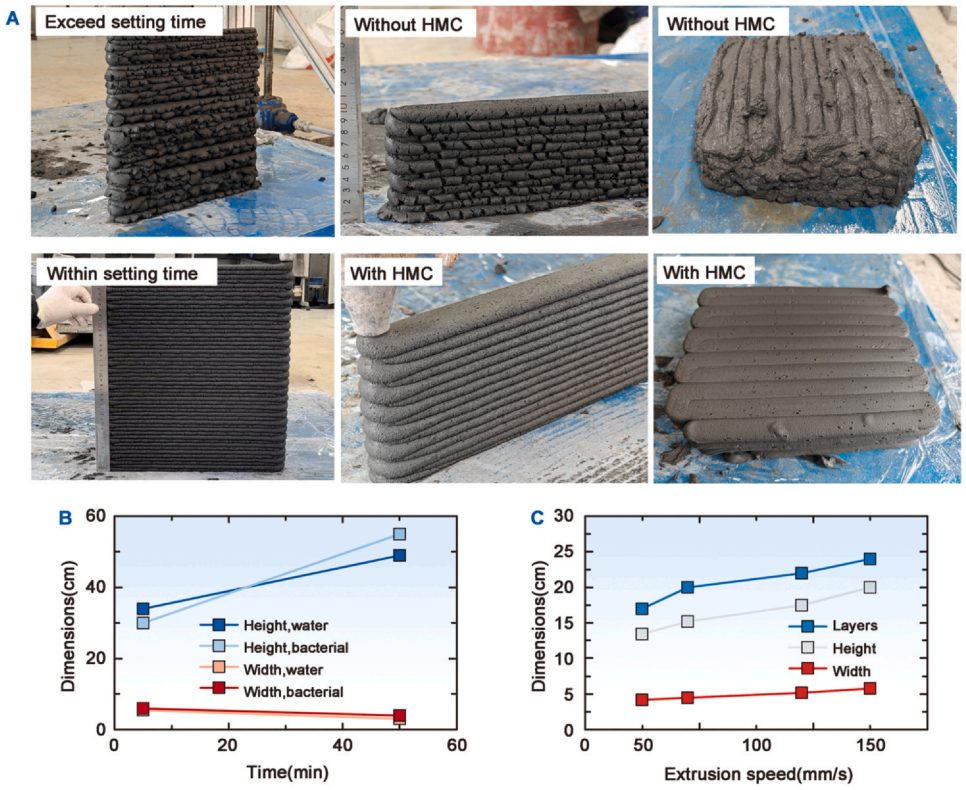


Fig. 5. Buildability of LRS Mortar: (**A**) Effect of HMC on building morphology of printed wall and brick; (B) Height and width of printed wall with resting time; (**C**) Height, width and layers of printed wall with extrusion speed.

improvement mechanism of cemented soils with magnesium oxide depends on the reaction between it with water and carbonate from bacterial hydrolysis. The produced magnesium carbonate hydrate plays dominated roles in bonding soil grains and improving the strength of the specimens (Wang et al. 2025). For water-based specimens, more product is in the form of brucite which exhibits lower strength than magnesium carbonate hydrate (Wang et al. 2025). This firstly explains why bacterial-based specimens own higher strength than the water-based specimens. Secondly, Ting et al. (2021) found that recycled glass aggregate can reduce the strength of 3D printing concrete and they explained that the surface of glass aggregate is smooth, which can decrease the adhesion between aggregate and binder and the interlayer

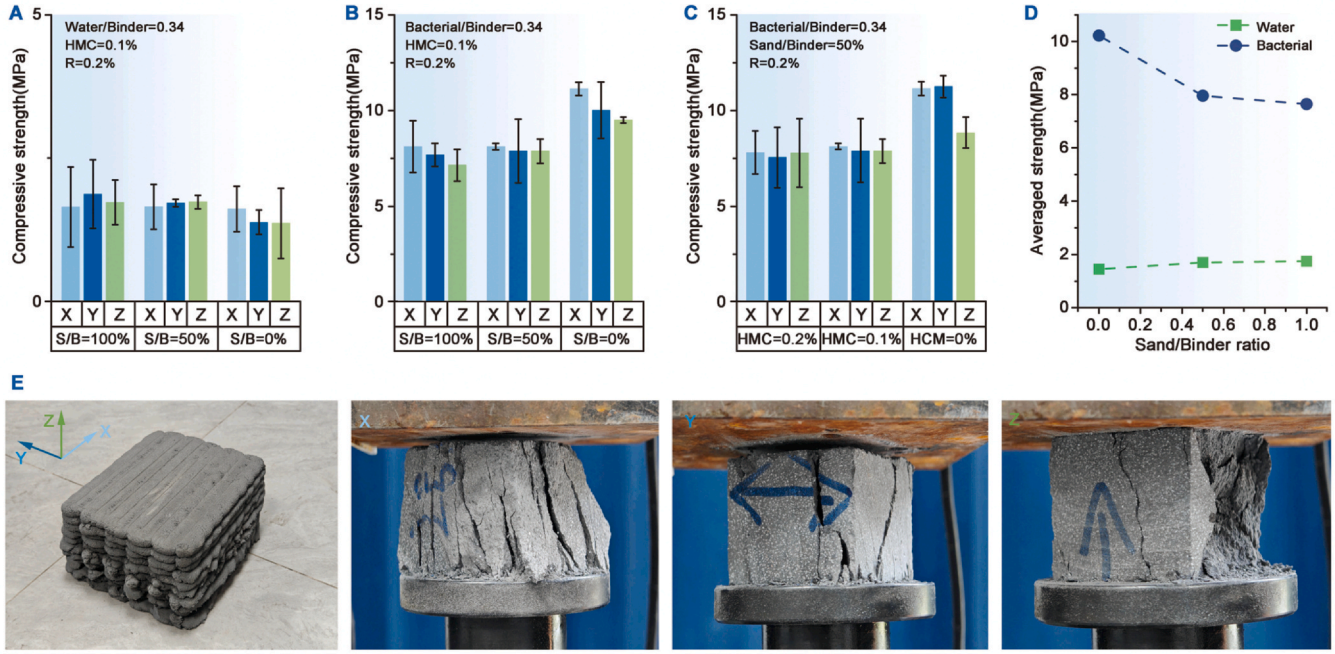


Fig. 6. Compressive strength of 3D printed specimens: (**A**) Effect of sand/binder ratio on compressive strength of water-based specimens; (**B**) Effect of sand/binder ratio on compressive strength of bacterial-based specimens; (**C**) Effect of HMC contents on compressive strength of bacterial-based specimens; (**D**) Comparison of averaged strength between two types of specimens; (**E**) Failure morphology of specimens along *X*, *Y* and *Z* directions.



Fig. 7. (**A–C**) SEM images of water-based and bacterial-based specimens; (**D**) 3D printed structures of lunar regolith simulant with biocarbonated MgO method.

bond strength. The sands used in this study is a machined sand and the surface is smoother than that of natural sand, which is probably the reason of the decreased strength with the bacterial-based specimens. For the water-based specimens, although the same sands were used. It is deduced that the binder strength is too low and the cohesion between aggregate and binder plays support the overall matrix. That means there is transition of the role of aggregate if the binder strength improves further. It is seen in Fig. 6A that the difference in strength of the specimens, induced by aggregate content, is not that large compared that of bacterial-based specimens. In the process of cutting printed blocks, the bacterial-based specimen without aggregate requires the most work for segmentation.

Fig. 6C shows the effect of HMC on the compressive strength of the printed specimens. It is seen that HMC has a negative effect on the strength development. Specially, for the specimens without HMC, their compressive strength is significantly higher than that with HMC. This phenomenon is inverse to the conclusions with respect to the effect of HMC in cement-based 3D printing concrete in Liu et al. (2023b). They showed that the addition of HMC can reduce the pores of printed specimens. However, Chen et al. (2020b) reported that there is an optimal value of HMC content for the limestone-calcined clay-based printing materials. For the mechanism of reduced strength, the weakening of interlayer connection with the addition of HMC could be one. For this study, HMC might hinder the reaction of MgO carbonation since the degree of freedom of carbonate in the solution with higher viscosity is lower than in aqueous solution.

Strength anisotropy of 3D printing concrete has been extensively reported in prior studies, which is caused by the different adhesion strength of layers in *X*, *Y*, and *Z* directions. Here, we defined *X* as the printing direction, *Z* is the upward direction and *Y* is the direction perpendicular to the other two directions. Normally, the stress in *X* direction is the highest since the loading along *X* direction can not cause interface shear failure caused by the slip of interface in the printed block (Xiao et al. 2021). In this study, no significant compressive strength anisotropy was observed. The compressive strength along *X* and *Y* directions is mostly higher than that along Z direction. The lower Z strength is attributed to that the bond strength between the lateral interfaces (deposition surface) is weaker than that between the vertical interfaces. Fig. 6E shows the failure pattern of the segmented specimens. The fracture surfaces were generated along the interface direction for the X loading specimens. For the other loading directions, the fracture shows the pattern of peeling and the surfaces are not that regular. This observation is similar with the failure pattern reported in (Aminpour and Memari, 2025). The microscopic images of printed specimens are shown in Fig. 7(A–C). The crystal of brucite and hydromagnesite can be found in the water-based and bacterial-based specimens, respectively, which is similar with the findings in Shi et al. (2024). However, the crystal size is smaller compared with that shown in Shi et al. (2024). This may be caused by the content of MgO and the additives used in the 3D printing mortar, which needs to be further studies with the smaller scale tests.

4. Discussion

The results in this paper showed the possibility of 3D-printing lunar regolith with the binder of MgO and bacterial-based solution. It is found that the maximum compressive strength can reach over 11 MPa for the group of pre-hydrolyzed urea with bacterial. This strength is over 6 times of the compressive strength of the specimens made with MgO and water, indicating the excellent ability of the biocarbonation routine for lunar regolith 3D printing. Fig. 7 D shows printed components with biocarbonated MgO method with the mass ratio of 20% and it can bear a certain of loading. It is also found in this paper that for the pure lunar regolith, it is difficult to perform high-quality 3D printing due to its coarse fraction and low water retention ability. The additives or changing the gradation of lunar regolith is necessary to guaranine flowability and buildability. The additives, such as retarder and thickener, should be sourced from nature. This is important since the in-situ regeneration of these materials on the Moon is the requirement for keeping living sustainability and reducing the cost of transportation. Biobased materials, such as citric acid and alginate, could be the

options. Future studies could be conducted to investigate the types of bio-additives for lunar regolith 3D printing and their effects on the biocarbonation process. Besides, in this paper, only 20% MgO was used. This is not a high dosage, which leads to a low reinforcement strength compared with alkali-activated and sintered lunar regolith (Han et al., 2022; Ma et al., 2023). Shi et al. (2024) reported that for mold casted lunar regolith with biocarbonated MgO, a dosage larger than 10% leads

to a lower biocarbonation rate but the strength still increases with the improvement of MgO content. In future study, 3D printing with higher dosages of MgO will be studied to investigate the effects of MgO content on the biocarbonation performance. The influence of lunar regolith simulant quality will also be considered in upcoming tests.

5. Conclusion

This paper investigates the additive manufacturing of lunar regolith with biocarbonated magnesium oxide. The effects of solution type, thickener, and aggregate on the flowability, buildbility, green strength and compressive strength are studied. The following conclusions can be summarized. A lunar regolith simulant was prepared, which owns similar particle size gradation and chemical component with the lunar soils of Chang'e-5. the flow diameters of the mortars with bacterial solution are significantly higher than those prepared with water. With the addling of HMC, the flow diameter significantly decreases from 20.5 cm to 13.75 cm. Retarder can extend the setting time of the biocarbonated MgO mortar and the flow diameter changes from 18.3 cm to 10.5 cm with the content of retarder increases to 0.2%. Green strength increases from 0.12 MPa to 2.11 MPa from 50th min to 240th min for bacterial-based solution. For water-based solution, the green strength is 0.3 MPa at the 240th min. The buildibility can be significantly improved with the addition of HMC. For bacterial-based solutions, the maximum peak compressive strength of the printed specimens is 11.25 MPa which is significantly higher than 1.88 MPa of the maximum strength of water-based specimens. The compressive strength slightly increases with the increase of sand/binder ratio for water-based specimen. However, the trend is inverse for bacterial-based solution and the averaged strength drops from 10.22 MPa to 7.65 MPa with the sand/binder ratio changes from 0% to 100%.

CRediT authorship contribution statement

Hanlong Liu: Writing – review & editing, Methodology, Investigation, Funding acquisition, Conceptualization. **Yang Xiao:** Writing – review & editing, Conceptualization. **Jinquan Shi:** Writing – original draft, Methodology, Investigation, Formal analysis, Conceptualization. **Baofeng Cao:** Formal analysis. **Junbo Sun:** Resources. Baofeng Cao: Formal analysis.

Declaration of Competing Interest

Hanlong Liu is the Editor-in-chief for *Biogeotechnics*, Yang Xiao is the Executive Deputy Editor-in-Chief for *Biogeotechnics* and Jinquan Shi is the Associate Editor for *Biogeotechnics*, they were not involved in the editorial review or the decision to publish this article. The other authors declare that they have no known competing financial interests or personal relationships that could have appeared to influence the work reported in this paper.

Acknowledgement

We would like to acknowledge the assistance from Dr. Xin Yang and Mr. Zhuowen Yan in test preparation. The financial support of testing equipment and materials from the Institute for Smart City of Chongqing University in Liyang is greatly appreciated.

References

Aminpour, N., & Memari, A. (2025). Analysis of anisotropic behavior in 3d concrete printing for mechanical property evaluation. *Journal of Building Engineering, 99*, Article 111652. https://doi.org/10.1016/j.jobe.2024.111652

Bai, G., Wang, L., Ma, G., Sanjayan, J., & Bai, M. (2021). 3D printing eco-friendly concrete containing under-utilised and waste solids as aggregates. *Cement and Concrete Composites, 120*, Article 104037. https://doi.org/10.1016/j.cemconcomp.2021.104037

Bao, C., Zhang, D., Wang, Q., Cui, Y., & Feng, P. (2024). Lunar in situ large-scale construction: Quantitative evaluation of regolith solidification techniques. *Engineering, 39*, 204–221. https://doi.org/10.1016/j.eng.2024.03.004

Bao, C., Wang, Y., Pearce, G., Zhao, P., Liu, M., & Mushtaq, R. T. (2025). 3D printing of regolith-based epoxy composites with excellent temperature resistance and mechanical strength. *Acta Astronautica, 229*, 787–803. https://doi.org/10.1016/j.actaastro.2025.02.001

Benaroya, H., Bernold, L., & Chua Koon, M. (2002). Engineering, design and construction of lunar bases. *Journal of Aerospace Engineering, 15*(2), 33–45. https://doi.org/10.1061/(ASCE)0893-1321(2002)15:2(33)

Buj, I., Torras, J., Casellas, D., Rovira, M., & Pablo, J. De (2009). Effect of heavy metals and water content on the strength of magnesium phosphate cements. *Journal of Hazardous Materials, 170*(1), 345–350. https://doi.org/10.1016/j.jhazmat.2009.04.091

Chen, M., Li, L., Wang, J., Huang, Y., Wang, S., Zhao, P., Lu, L., & Cheng, X. (2020a). "Rheological parameters and building time of 3d printing sulphoaluminate cement paste modified by retarder and diatomite. *Construction and Building Materials, 234*, Article 117391. https://doi.org/10.1016/j.conbuildmat.2019.117391

Chen, Y., Chaves Figueiredo, S., Li, Z., Chang, Z., Jansen, K., Çopuroğlu, O., & Schlangen, E. (2020b). "Improving printability of limestone-calcined clay-based cementitious materials by using viscosity-modifying admixture.". *Cement and Concrete Research, 132*, Article 106040. https://doi.org/10.1016/j.cemconres.2020.106040

Cocks, F. H., Klenk, P. A., Watkins, S. A., Simmons, W. N., Cocks, J. C., Cocks, E. E., & Sussingham, J. C. (2002). Lunar ice: adsorbed water on subsurface polar dust. *Icarus, 160*(2), 386–397. https://doi.org/10.1006/icar.2002.6972

Crawford, I. A., Anand, M., Cockell, C. S., Falcke, H., Green, D. A., Jaumann, R., & Wieczorek, M. A. (2012). Back to the moon: the scientific rationale for resuming lunar surface exploration. *Planetary and Space Science, 74*(1), 3–14. https://doi.org/10.1016/j.pss.2012.06.002

Dikshit, R., Dey, A., Gupta, N., Varma, S. C., Venugopal, I., Viswanathan, K., & Kumar, A. (2021). Space bricks: from lss to machinable structures via micp. *Ceramics International, 47*(10, Part B), 14892–14898. https://doi.org/10.1016/j.ceramint.2020.07.309

Ding, C., Li, Q., Xu, J., Lei, Z., Li, J., Su, Y., & Huang, S. (2023). Moon-based ground penetrating radar derivation of the helium-3 reservoir in the regolith at the Chang'e-3 landing site. *IEEE Journal of Selected Topics in Applied Earth Observations and Remote Sensing, 16*, 2764–2776. https://doi.org/10.1109/JSTARS.2023.3253499

Ellery, A. (2021). Leveraging in situ resources for lunar base construction. *Canadian Journal of Civil Engineering, 49*(5), 657–674. https://doi.org/10.1139/cjce-2021-0098

Ge, C., Feng, X., Xu, D., Liu, K., An, A. K., & Fang, J. (2025). Exploring solar-powered water treatment in outer space: technologies, challenges, and opportunities for sustainable space habitats. *Space Habitation, 1*(1), Article 100006. https://doi.org/10.1016/j.spaceh.2025.100006

Han, W., Ding, L., Cai, L., Zhu, J., Luo, H., & Tang, T. (2022). Sintering of hust-1 lunar regolith simulant. *Construction and Building Materials, 324*, Article 126655. https://doi.org/10.1016/j.conbuildmat.2022.126655

Indyk, S. J., & Benaroya, H. (2017). A structural assessment of unrefined sintered lunar regolith simulant. *Acta Astronautica, 140*, 517–536. https://doi.org/10.1016/j.actaastro.2017.09.018

Li, C., Hu, H., Yang, M. F., Pei, Z. Y., Zhou, Q., Ren, X., ... Ouyang, Z. (2022). Characteristics of the lunar samples returned by the chang'e-5 mission. *National Science Review, 9*(2), https://doi.org/10.1093/nsr/nwab188

Li, L., Yu, H., Dong, J., Ma, H., Yu, W., Fang, K., ... Li, W. (2025). Optimal selection of magnesium phosphate cement systems for lunar soil concrete: potassium, ammonium, calcium, and sodium magnesium phosphate cements. *Advances in Space Research, 75*(6), 5205–5226. https://doi.org/10.1016/j.asr.2024.12.059

Li, Z., Wang, L., & Ma, G. (2018). Method for the enhancement of buildability and bending resistance of 3d printable tailing mortar. *International Journal of Concrete Structures and Materials, 12*(1), 37. https://doi.org/10.1186/s40069-018-0269-0

Liu, X., Xiao, J., Cai, D., Su, Q., Yang, G., Yuan, S., & Jiang, G. (2023a). "Recent advances in subgrade engineering for high-speed railway. *Intelligent Transportation Infrastructure, 2*. https://doi.org/10.1093/iti/liad001

Liu, Y., Wang, L., Yuan, Q., & Peng, J. (2023b). "Effect of coarse aggregate on printability and mechanical properties of 3d printed concrete. *Construction and Building Materials, 405*, Article 133338. https://doi.org/10.1016/j.conbuildmat.2023.133338

Liu, Z., Qin, Y., Hu, C., & Wang, F. (2024). Boosting mgo hydration through sodium bicarbonate: enhancing the strength of mgo-calcined clay cementitious materials. *Journal of Building Engineering, 98*, Article 111279. https://doi.org/10.1016/j.jobe.2024.111279

Ma, S., Akca, A. H., Esposito, D., & Kawashima, S. (2020). Influence of aqueous carbonate species on hydration and carbonation of reactive mgo cement. *Journal of CO2 Utilization, 41*, Article 101260. https://doi.org/10.1016/j.jcou.2020.101260

Ma, S., Jiang, Y., Fu, S., He, P., Sun, C., Duan, X., ... Zhou, Y. (2023). 3D-printed lunar regolith simulant-based geopolymer composites with bio-inspired sandwich architectures. *Journal of Advanced Ceramics, 12*(3), 510–525. https://doi.org/10.26599/JAC.2023.9220700

Meurisse, A., Makaya, A., Willsch, C., & Sperl, M. (2018). Solar 3D printing of lunar regolith. *Acta Astronautica, 152*, 800–810. https://doi.org/10.1016/j.actaastro.2018.06.063

Meurisse, A., Beltzung, J. C., Kolbe, M., Cowley, A., & Sperl, M. (2017). Influence of mineral composition on sintering lunar regolith. *Journal of Aerospace Engineering, 30*(4), 04017014. https://doi.org/10.1061/(ASCE)AS.1943-5525.0000721

T. Nakamura B. Smith Solar thermal system for lunar isru applications: Development and field operation at mauna kea, hi Proc., 49th AIAA Aerospace Sciences Meeting including the New Horizons Forum and Aerospace Exposition 433.

Neves, J. M., Ramanathan, S., Suraneni, P., Grugel, R., & Radlińska, A. (2020). Characterization, mechanical properties, and microstructural development of lunar regolith simulant-portland cement blended mixtures. *Construction and Building Materials, 258*, Article 120315. https://doi.org/10.1016/j.conbuildmat.2020.120315

Nie, J., Cui, Y., Senetakis, K., Guo, D., Wang, Y., Wang, G., ... Li, A. (2023). Predicting residual friction angle of lunar regolith based on Chang'e-5 lunar samples. *Science Bulletin, 68*(7), 730–739. https://doi.org/10.1016/j.scib.2023.03.019

Nie, J., Wang, S., Cui, Y., Wu, Z., He, J., Wang, G., & Zeng, X. (2025). Analyzing the mechanical heterogeneity of the Chang'e-5 lunar breccia clast: implications for the elastic modulus of lunar rock. *Journal of Geophysical Research: Planets, 130*(6), https://doi.org/10.1029/2024JE008849

Osio-Norgaard, J., Hayes, A. C., & Whiting, G. L. (2021). Sintering of 3D printable simulated lunar regolith magnesium oxychloride cements.". *Acta Astronautica, 183*, 227–232. https://doi.org/10.1016/j.actaastro.2021.03.016

Papike, J. J., Simon, S. B., & Laul, J. C. (1982). The lunar regolith: chemistry, mineralogy, and petrology. *Reviews of Geophysics, 20*(4), 761–826. https://doi.org/10.1029/RG020i004p00761

Pederson, F., Ellersick, L., & Kim, H. J. (2025). A review of lunar regolith based alkali activated materials and sintered regolith for use as a construction material. *Acta Astronautica, 232*, 502–515. https://doi.org/10.1016/j.actaastro.2025.03.032

Reiter, L., Wangler, T., Roussel, N., & Flatt, R. J. (2018). The role of early age structural build-up in digital fabrication with concrete. *Cement and Concrete Research, 112*, 86–95. https://doi.org/10.1016/j.cemconres.2018.05.011

Scott, A., Oze, C., Shah, V., Yang, N., Shanks, B., Cheeseman, C., ... Watson, M. (2021). Transformation of abundant magnesium silicate minerals for enhanced CO_2 sequestration. *Communications Earth Environment, 2*(1), 25. https://doi.org/10.1038/s43247-021-00099-6

Shahsavari, M. H., Karbala, M. M., Iranfar, S., & Vandeginste, V. (2022). Martian and lunar sulfur concrete mechanical and chemical properties considering regolith ingredients and sublimation. *Construction and Building Materials, 350*, Article 128914. https://doi.org/10.1016/j.conbuildmat.2022.128914

She, X., Wang, J., Xu, W., & Xiao, L. (2025). Research on the impact of extraterrestrial lava tube environments on human survival and countermeasures. *Space Habitation, 1*(1), Article 100002. https://doi.org/10.1016/j.spaceh.2024.100002

Shi, J., Xiao, Z., Xiao, Y., & Liu, H. (2024). Bio-molding of lunar regolith with bio-carbonized magnesium oxide. *Biogeotechnics*Article 100159. https://doi.org/10.1016/j.bgtech.2024.100159

Shoaei, P., Gallantree-Smith, H., Martínez Pacheco, V., Pamies, R., Kjøniksen, A. L., & Pilehvar, S. (2024). Comparative analysis of 3D printing of portland cement mortars with hydroxypropyl methylcellulose and microfibrillated cellulose as viscosity modifying agents. *Materials Design, 244*, Article 113124. https://doi.org/10.1016/j.matdes.2024.113124

Song, L., Xu, J., Tang, H., Liu, J., Liu, J., Li, X., & Fan, S. (2020). Vacuum sintering behavior and magnetic transformation for high-Ti type basalt simulated lunar regolith. *Icarus, 347*, Article 113810. https://doi.org/10.1016/j.icarus.2020.113810

Su, Y., Feng, J., Jin, P., & Qian, C. (2019). Influence of bacterial self-healing agent on early age performance of cement-based materials. *Construction and Building Materials, 218*, 224–234. https://doi.org/10.1016/j.conbuildmat.2019.05.077

Taylor, L. A., Pieters, C. M., & Britt, D. (2016). Evaluations of lunar regolith simulants. *Planetary and Space Science, 126*, 1–7. https://doi.org/10.1016/j.pss.2016.04.005

Ting, G. H. A., Tay, Y. W. D., & Tan, M. J. (2021). Experimental measurement on the effects of recycled glass cullets as aggregates for construction 3D printing. *Journal of Cleaner Production, 300*, Article 126919. https://doi.org/10.1016/j.jclepro.2021.126919

Tramontin Souza, M., Maia Ferreira, I., Guzi De Moraes, E., Senff, L., Arcaro, S., Castro Pessôa, J. R., ... Novaes De Oliveira, A. P. (2022). Role of chemical admixtures on 3d printed portland cement: Assessing rheology and buildability. *Construction and Building Materials, 314*, Article 125666. https://doi.org/10.1016/j.conbuildmat.2021.125666

Ulubeyli, S. (2022). Lunar shelter construction issues: the state-of-the-art towards 3D printing technologies. *Acta Astronautica, 195*, 318–343. https://doi.org/10.1016/j.actaastro.2022.03.033

Wang, D. L., Tang, C. S., Pan, X. H., Dong, Z. H., Wang, R., Zhang, J. Z., ... Shi, B. (2025). Construction and demolition waste stabilization through biocarbonation of reactive magnesia cement: Effect of urea concentration. *Journal of Materials in Civil Engineering, 37*(1), 04024450. https://doi.org/10.1061/JMCEE7.MTENG-17257

Warren, P., Raju, N., Ebrahimi, H., Krsmanovic, M., Raghavan, S., Kapat, J., & Ghosh, R. (2022). Effect of sintering temperature on microstructure and mechanical properties of molded martian and lunar regolith. *Ceramics International, 48*(23, Part B), 35825–35833. https://doi.org/10.1016/j.ceramint.2022.07.329

Xiao, J., Liu, H., & Ding, T. (2021). Finite element analysis on the anisotropic behavior of 3D printed concrete under compression and flexure. *Additive Manufacturing, 39*, Article 101712. https://doi.org/10.1016/j.addma.2020.101712

Xiao, Y., Stuedlein Armin, W., Ran, J., Evans, T. M., Cheng, L., Liu, H., ... Chu, J. (2019). Effect of particle shape on strength and stiffness of biocemented glass beads. *Journal of Geotechnical and Geoenvironmental Engineering, 145*(11), 06019016. https://doi.org/10.1061/(ASCE)GT.1943-5606.0002165

Zhang, H., Zhang, X., Zhang, G., Dong, K., Deng, X., Gao, X., Yang, Y., Xiao, Y., Bai, X., Liang, K., Liu, Y., Ma, W., Zhao, S., Zhang, C., Zhang, X., Song, J., Yao, W., Chen, H., Wang, W., Zou, Z., & Yang, M. (2021a). "Size, morphology, and composition of lunar samples returned by chang'e-5 mission. *Science China Physics, Mechanics Astronomy, 65*(2), Article 229511. https://doi.org/10.1007/s11433-021-1818-1

Zhang, X., Gholami, S., Khedmati, M., Cui, B., Kim, Y.-R., Kim, Y.-J., Shin, H.-S., & Lee, J. (2021b). "Spark plasma sintering of a lunar regolith simulant: effects of parameters on microstructure evolution, phase transformation, and mechanical properties. *Ceramics International, 47*(4), 5209–5220. https://doi.org/10.1016/j.ceramint.2020.10.100

Zheng, Y., Ouyang, Z., Li, C., Liu, J., & Zou, Y. (2008). China's lunar exploration program: present and future. *Planetary and Space Science, 56*(7), 881–886. https://doi.org/10.1016/j.pss.2008.01.002

Zhou, C., Li, X., Gao, Y., & Chen, R. (2025). Parametric design and optimization for lava tubes-like lunar arch habitation with large span. *Space Habitation, 1*(1), Article 100001. https://doi.org/10.1016/j.spaceh.2024.100001

Zhou, C., Chen, R., Xu, J., Ding, L., Luo, H., Fan, J., ... Tang, B. (2019). In-situ construction method for lunar habitation: Chinese super mason. *Automation in Construction, 104*, 66–79. https://doi.org/10.1016/j.autcon.2019.03.024

China National Standards GB/T 2419-2005, Test method for fluidity of cement mortar, Beijing, China (in Chinese).